LOAD DEFORMATION RESPONSE OF CONCRETE HAVING ALTERNATE REINFORCEMENT FORMS

HIMANSHU[*], BISWAJIT PAL[†] AND ANANTH RAMASWAMY[*]

[*] Indian Institute of Science, Department of Civil Engineering, Bangalore, Karnataka 560012, INDIA
e-mail: himanshu1@iisc.ac.in ; ananth@iisc.ac.in;

[†] Central Building Research Institute, Roorkee, Uttarakhand 247657, INDIA
e-mail: biswajitjgec.1992@gmail.com

Key words: Cohesive fracture, Fiber Reinforced Concrete, Composites, Durability

Abstract: Steel rebar has been an effective and cost-efficient reinforcement for concrete. Corrosion in reinforcements has led to exploring alternate reinforcements such as FRP rebars, hybrid steel core FRP wound GFRP strands rebar and short fiber (steel and polyester, polypropylene, etc) for its effectiveness as a reinforcement to arrest crack initiation and growth and enhancing ductility. The present study reports on the effectiveness of hybrid rebar as a reinforcement in fiber reinforced concrete beams. Thereafter a quasi-brittle phase field-based damage model for short fiber reinforced composites is developed to investigate the effectiveness of fibers in the concrete matrix in providing bridging action needed to enhance the ductility. Steel fiber reinforced concrete (SFRC) is employed as a case study. The model incorporates randomly distributed steel fibers within a macroscale concrete matrix, with fibers represented as two-dimensional truss elements. A traction-separation law governs the fiber-concrete interface, while the concrete matrix is modelled using a quasi-brittle phase field damage approach. The model effectively simulates the classical three-point bending test for SFRC demonstrating good agreement with experimental data. Due to the macroscale representation of the concrete matrix, the model it is possible to extend its application to high-strength steel fiber reinforced concrete (HS-SFRC) by adjusting material properties of concrete. Moreover simulation of complex loading conditions can also be effectively simulated. Results of such simulations carried out will be shown during the presentation.

1 INTRODUCTION

Concrete is a common building material that is also being used for the construction of important structures such as bridges, tall buildings, dam structures, offshore structures, etc. Concrete has a high compressive strength, low tensile strength, and brittle failure characteristics. The use of steel bars as reinforcement in tension zone and prestressing of concrete structural sections are methods used to circumvent the low tensile strength and brittle behavior of the concrete. However, these methods do not improve the inherent tensile strength and the brittle behavior of the concrete. In the conventional approach of design of reinforced concrete structures, the compressive strength of the concrete is accounted for while the tensile strength of the concrete is neglected. Composite materials such as glass fiber reinforced polymer (GFRP) and carbon fiber reinforced polymer (CFRP) have become an attractive alternative to steel reinforcement, as these materials are non-corrosive, possesses a high strength-to-weight ratio and are commercially available for the construction industry [1, 2]. In FRP rebar reinforced beams the use of fibers as an additive in the concrete matrix to enhance the cross-sectional ductility and to improve shear resistance has also been explored in earlier studies [3, 4]. In this study, the hybrid rebars used consisted of ten 2 mm-diameter GFRP

strands, helically wound bonded on a 6 mm-diameter steel rod, with the help of an epoxy binder material ensuring that there is no gap between the GFRP strands through-out the length of the rebar. In earlier studies bond between the FRP reinforcement and concrete was achieved using sand coating on the surface of the rebars [4] or through a secondary surface treatment of the rebars [1, 4]. It is expected that the helical winding in hybrid bars would offer adequate bond through interlocking. The principal advantage of hybrid rebar over the FRP rebar is the ductility introduced into the cross section due to the presence of steel. The stress-strain curve of the hybrid rebar is similar in shape to that of steel rebar. In this study, an attempt is made to study the behaviour of hybrid rebar reinforced beams, which are designed as under-reinforced section like design principles employed for conventional steel reinforced concrete beams.

The inability to prevent the propagation of micro-cracks, which originate at inherent flaws in the concrete results in the formation and propagation of cracks unstably even at low tensile stresses. Efforts to improve the tensile strength of the brittle materials lead to the concept of two-phase materials in which the presence of one phase improves the basic properties of the other phase. Fiber reinforced concrete is a two-phase material in which the chopped steel fibers bridge across the inherent micro-cracks in the concrete matrix and controls the propagation of the crack. Use of fibers in reinforced concrete structures increases the strength and reduces the crack widths. However, the interfacial transition zone (ITZ) between cement pastes and aggregate remains a vulnerable region within concrete. When subjected to external loads, the ITZ is more susceptible to tensile failure due to its inherent weakness [5]. Therefore, to improve the performance of concrete under tensile loading, fibers (e.g., steel, carbon etc.) are generally added in the concrete mix. The fibers in steel fiber reinforced concrete (SFRC) usually al- lows concrete to sustain more tensile load by bridging the cracks. Such enhanced tensile or flexural capacity of SFRC is strongly dependent on the types and aspect ratios of the fibers. For instance, based on the experimental works,

Earlier investigations by Hughes (1981)[6], Narayanan and Kareem-Palanjian (1984)[7], Narayanan and Darwish (1987)[8], Balaguru and Ezeldin (1987)[9], Wafa et al. (1992)[10], Tan et al. (1995)[11], diPrisco and Gambarova (1995)[12], Furlan and Hanai (1999)[13], Abdul-Wahab and Al-Kadhimi (2000) [14], Padmarajaiah and Ramaswamy (2001) & (2002))[15-16], Job Thomas and Ramaswamy [17] and Tan et al. (2002) [18] indicated that addition of steel fibers over entire cross section improves the flexural and shear resisting characteristics of structural concrete elements. The investigations by Chern et al. (1992) [19] indicated that the addition of fibers affects failure surface of the concrete. The addition of fibers increases the strength and alters the post-peak softening properties of the concrete. The improvement in the strength properties is due to the confining action offered by the discrete randomly oriented steel fibers in the concrete matrix. The variation in the post-peak response of the stress-strain characteristic curve is due to the bridging of the steel fibers across the crack in the concrete. The lack of proper analysis and design methods for steel fiber reinforced concrete has limited its widespread application. The high cost and time demand associated with the experimental works have driven re- searchers to increasingly explore empirical, numerical, and analytical modeling techniques for SFRC (including other fibers). To evaluate the effective elastic characteristics of composite materials, several analytical homogenization techniques have been developed. These techniques aim to replace a heterogeneous material (composed of different phases) with a homogeneous continuum for simpler analysis. Analytical homogenization methods, such as the Hashin-Shtrikman bounds [20] and the Voigt-Ruess bounds [21], focus on estimating upper and lower bounds for the effective properties. Building upon Eshelby's foundational work along with the equivalent inclusion technique [22], researchers have developed a diverse range of advanced analytical homogenization models [23]. These

models encompass the Mori-Tanaka approximation [24], the double inclusion model [25], the generalized self-consistent model, and the self-consistent approximation model [26]. Building on the concept of Mori-Tanaka [24], a Representative Volume Element (RVE) for SFRC was homogenized considering random fiber orientation and periodic boundary conditions [27].

To accurately predict the behavior of SFRC under various loading conditions, a comprehensive understanding of the underlying fracture mechanisms is essential. The experimental studies have shown that fiber matrix interactions have an initial linear elastic response followed by micro-cracking and coalescence, fiber bridging action and eventually pullout at bond failure. Interfacial load transfer between steel fibers and the concrete matrix is a critical aspect governing the performance of SFRC. Deng et al. [28] experimentally investigated the fiber matrix interaction in the case of fiber-reinforced concrete by studying the fiber pull-out behavior of a single fiber. The experimental observation revealed that the interfacial bond-slip response depends on both the fiber type (straight or hooked) and its aspect ratio. By leveraging these experimental observations, the authors developed a model for the interfacial bond-slip behavior between fibers and the concrete matrix. Bitencourt Jr. et al. [29] proposed a finite element (FE)-based numerical model that explicitly modeled individual fibers in the concrete matrix. In the model [29], constitutive behavior of concrete was described through a continuum damage mechanics (CDM) based formulation proposed by Cervera et al. [30]. A cohesive zone type behavior was employed to describe the bond-slip behavior between fibers and the surrounding concrete interface [31]. The application of the model was further extended in [32] to evaluate the post-cracking parameters according to EN 14651 for application of SFRC as structural material.

This study presents a numerical modelling framework for simulating the fracture behavior of SFRC, incorporating a phase-field approach to capture the crack initiation and propagation

within the concrete matrix. The model adopts a multi-scale-based modeling framework to explicitly represent individual fibers within the macro-scale concrete domain along with a bond-slip law to represent the fiber-matrix interaction. Since the concrete matrix is modeled at the macro-scale, the developed model offers flexibility in simulating different concrete types, ranging from normal to high-strength concrete, by adjusting material properties. Consequently, the model's applicability extends to high-strength concrete, enabling the investigation of high-strength SFRC behavior. The developed model is afterwards applied to simulate three-point bending tests for both normal and high-strength SFRC, demonstrating good agreement with experimental load-displacement curves and crack patterns. The proposed approach offers insights into the critical fiber-level mechanisms, such as fiber bridging and pull-out, contributing to a deeper understanding of SFRC fracture behavior. The model's ability to capture essential aspects of SFRC behavior is further demonstrated through simulations involving complex loading conditions, such as those encountered in mixed-mode scenario. A critical review of the literature reveals that majority of the existing damage models for SFRC primarily rely on CDM or damage plasticity law for concrete [33]. While these approaches offer valuable insights, the existing models have several limitations. A significant challenge in utilizing damage plasticity models for concrete is the accurate determination of input parameters like yield stress and yield criteria [33]. These parameters are often difficult to obtain through experimental procedures and can vary considerably depending on the concrete type (normal vs. high strength) [34]. This limitation restricts the model's applicability to a specific concrete mix. Furthermore, existing models often struggle to capture the high ductility behavior observed near the peak load in load-deflection curves in SFRC, particularly when the fiber content is greater or equal to 1% [35]. Addressing these limitations is crucial for developing more robust and versatile SFRC models especially to emphasize on post-peak

behavior. This research presents a unified modeling framework for simulating the fracture behavior of Steel Fiber Reinforced Concrete (SFRC) under various loading conditions, encompassing both normal and high-strength concrete mixes. A primary objective is to accurately simulate the high post-peak ductility behavior observed in SFRC specimens with fiber contents approaching 1% as reported in experiments [35-37].

In this study a multi-scale modeling approach for SFRC is developed. The concrete matrix is modeled at macro-scale using a quasi-brittle phase field (PF) damage model [38]. Whereas fibers are explicitly modeled as linear truss element. The interface between concrete and each fiber is modelled using a bond-slip law [31]. The damage model of concrete incorporates a smeared scalar damage field variable that evolves throughout the deformation process, enabling the simulation of crack initiation, propagation, and material degradation. The PF model [39] has been successfully extended to capture the behavior of quasi-brittle materials like concrete at macro [34] and mesoscale [40]. The models robustness allows for the application of the PF model even at the meso-scale for detailed simulations [41]. Additionally, unlike conventional damage models, the PF framework provides a differential equation governing the damage evolution. This feature facilitates the straightforward incorporation of multi-physics phenomena into the modeling framework [42-44]. The quasi-brittle phase field (PF) damage model requires three key parameters to simulate fracture in concrete: tensile strength (f_t), fracture energy release rate (G_c), and characteristic length scale (l_0). The l_0 defines the effective width over which crack damage is smeared within the finite element mesh. For concrete, a value of 5-10 mm is typically employed [38]. In contrast, f_t and G_c can be readily obtained through experimental procedures like three- point bending or notched beam tests [35, 37]. This advantage allows the proposed PF model to be applicable to a wide range of concrete types, including normal and high-strength concretes. By incorporating these material properties, the proposed model achieves a level of unification that transcends the limitations of specific concrete mixes. A three-point bending fracture behavior of SFRC has been simulated. Other example problems having complex loads will be shown during the oral presentation.

2.0 METHODOLOGY

Tests were conducted to determine the mechanical properties of the hybrid bars and the GFRP coupon taken from the GFRP stirrup. The hybrid bar had an ultimate tensile strength of 647MPa with a corresponding ultimate strain of 0.014876 and a modulus of elasticity of 101988MPa. The GFRP coupon had an ultimate tensile strength of 191MPa at an ultimate strain of 0.01542. The modulus of elasticity of the GFRP coupon was 13310MPa. A pullout test was conducted to determine the bond stress of hybrid bars. The pullout specimen consisted of 152 mm by 304 mm concrete cylinder with a hybrid rebar embedded axisymmetically with an embedment length of 200 mm. Bond stress (τ_{bond}) at failure was found to be 3.3MPa.

The experimental work included testing of a set of three beam specimens with moderately high strength concrete (48 MPa) under four point bending loads. The size of the beam was 180 x 250 x 1540 mm. Shear span and the pure moment span of the beam specimens were 420 mm and 500 mm, respectively. The specimens consisted of three- flexure control beams of which one beam specimen (beam 1) had steel as longitudinal (2 12mm and 2 10mm dia rebars) and transverse reinforcement (8mm 2 leg ties at 120mm c/c) and the other two were with hybrid rebar as longitudinal reinforcement (3 10.8mm dia bars) and GFRP stirrups (20mmx5.5mm bar section at 120mm c/c). All the beam specimens were designed as under-reinforced section. Further, the design assumed that the stress in the rebars at failure would reach its ultimate stress. One of the beams (beam 3) was cast using 0.1% by weight of cement of polypropylene fibers introduced into the concrete matrix. All the beam specimens were tested as simply supported members subjected to four-point loading. Strain gages were fixed to the hybrid rebars and steel longitudinal bars at mid-span. Strain

gages were also fixed to the surface of the concrete in the flexure zone. Linear Variable Differential Transducers (LVDT) and digital dial gages were used to measure the vertical displacement at mid-span and quarter-span of each specimen.

Hybrid rebar reinforced concrete beams have been designed assuming that perfect bond exists between rebar and surrounding concrete until the failure of the beam. The flexural capacity of the beam has been estimated based on the premise that the limiting strain in the extreme compression fiber of concrete ($\varepsilon_{c,lim}$ = 0.003) and the ultimate tensile strain in the hybrid rebar ($\varepsilon_{hyb,ult.}$= 0.015) will reach simultaneously. The target design load of beam 1 was 197kN and Beam 2 & 3 181kN.

During the fabrication of SFRC, the mixing process results in a random distribution of fibers with varying orientations. However, existing research suggests that the geometry and size of the mold influence the fibers alignment, with approximately over 50% of fibers align along the longitudinal axis in the case of beams and slabs [46]. Additionally, the volume fraction and size of coarse aggregate, along with the aspect ratio of the fibers have been shown to impact fiber orientation within the concrete matrix [47]. However, explicitly modeling coarse aggregate alongside individual fibers in a 3D concrete mix is computationally expensive. A multi-scale approach with the concrete matrix itself is modeled at the macro-scale for efficiency is employed in this study.

Given the computational challenges associated with solving a full 3D fracture problem, this study leverages a plane stress simplification. This approach approximates the 3D behavior by assuming a negligible out-of-plane stress component, which is a valid assumption for beams subjected to in-plane bending as in a three-point bending test. As our focus lies on planar beams, this simplification allows for an efficient representation of the 3D geometry. However, it's important to acknowledge that projecting the 3D fibers onto the 2D plane can lead to fiber intersections.

The planar body is discretized using four-node linear quadrilateral elements, while the fibers are meshed with two-node linear elements. The interaction between fibers and concrete is defined through a bond-slip law. For elements (four-node) where no fiber nodes are present, fracture is governed by the quasi-brittle phase field fracture model. However, for quadrilateral elements that contain a fiber node, a similar phase field damage model is implemented, incorporating the additional stiffness of the fiber projected onto the element [48].

To simulate crack propagation within a 2D planar body a phase field damage variable d is introduced. The variable d ranges from 0 to 1, wherein d=0 implies a closed crack or intact material and d=1 is a complete local damage (d cannot be negative). Cracks are inherently discrete phenomena. However, to model them within the framework of continuum mechanics, the crack is mathematically distributed over a characteristic length scale(l_0).

The potential energy of the body neglecting body force can be written as:

$$\Pi = \Pi_e + \Pi_{frac} - \Pi_{ext} = \int_{\Omega} \Psi(\epsilon(u), d)ds + \int_{\Omega} G_c \gamma(d, \nabla d)ds - \int_{\partial \Omega_t} f.u \, da$$

(1)

Where Π_e denotes the strain energy stored under deformation and Π_{frac} represents the fracture energy. Π_{ext} is the work done by the external forces. Ψ represents the strain energy density function and it can split into multiplication of two functions as [39]:

$$\Psi(\epsilon, d) = w(d)\Psi_0(\epsilon)$$

(2)

where Ψ_0 is the strain energy density of the undamaged material. For linear elastic solid it can be written as:

$$\Psi_0(\epsilon) = \frac{1}{2}\sigma : \epsilon, \quad \sigma = \mathbb{C} : \epsilon$$

(3)

σ and ϵ is the stress and stain tensor, whereas C is fourth order isotropic elasticity tensor. w(d) in eq. (2) is the degradation function, reflects the progressive reduction in the material stiffness as the damage process evolves. w(d) should satisfy the following:

$$w(0) = 1, \quad w(1) = 0, \quad w'(1) = 0$$

(4)

The first two conditions define the

completely intact and fully broken states of the material at a point within the domain. The third condition ensures convergence of the damage evolution towards the fully damaged state. The form of w(d) is discussed in [38] and that of ψ(d,∇d) represents the fracture surface density function and the expression for γ is given in [39].

$$\gamma(d, \nabla d) = \frac{1}{c_\alpha}\left[\frac{1}{l_0}\alpha(d) + l_0|\nabla d|^2\right], \quad c_\alpha = 4\int_0^1 \sqrt{\alpha(x)}dx$$

(5)

α(d) is the function that governs the homogeneous evolution of damage field (d) distribution within the domain. cα is used to regularise the fracture energy. Equation (1) can be written as:

$$\Pi = \int_\Omega w(d)\Psi_0(\epsilon(u))ds + \int_\Omega G_c\frac{1}{c_\alpha}\left[\frac{1}{l_0}\alpha(d) + l_0|\nabla d|^2\right]ds - \int_{\partial\Omega_t} f.uda$$

(6)

Upon minimizing the potential energy in an arbitrary direction δu and δd we get equation (7) and (8)

$$\int_\Omega \sigma : \delta\epsilon ds - \int_{\partial\Omega_t} f.\delta uda = 0 \quad bc's \quad as \quad \begin{cases} u = \bar{u} & on \ \partial\Omega_u \\ \sigma.n = 0 & on \ \partial\Omega_t \end{cases}$$

(7)

$$\int_\Omega \delta w(d)\Psi_0 ds + \int_\Omega G_c\delta\gamma(d, \nabla d)ds = 0 \quad bc's \quad as \quad \nabla d.n = 0 \quad on \quad \Gamma \cup \partial\Omega$$

(8)

As previously established, Ψ_0 represents the internal strain energy density of the undamaged material. The first term in Eq. (8) governs the evolution of the damage variable, d. This term is driven by the total elastic energy stored per unit volume within the material, which encompasses both compressive and tensile components. However, to capture the fracture phenomenon that is primarily driven by tensile stresses, the energy contribution from the positive eigenvalues of the stress tensor is considered in Eq. (7). Conversely, the energy contribution associated with negative eigenvalues (compressive stresses) is assumed to be negligible in the context of fracture initiation [39]. Damage progression in materials is inherently an irreversible phenomenon. To capture this irreversibility within the phase field framework a history variable H is introduced. This variable plays a crucial role in tracking the accumulated damage within the material as deformation progresses

$$H(x, t) = max\left\{\Psi_0^t, \ \max_{s\in[0,t]}\Psi_0^+\right\}$$

(9)

t is the initial threshold in term of tensile strength f_t of the material. Physically, it means the damage will only initiate at a point when the principal eigen value of stress tensor exceeds the tensile strength. The final evaluation of damage can be written as eq (10).

$$\int_\Omega \delta w(d)Hds + \int_\Omega G_c\delta\gamma(d, \nabla d)ds = 0 \quad bc's \quad as \quad \nabla d.n = 0 \quad on \quad \Gamma \cup \partial\Omega$$

(10)

Eq. (7) and (10) are coupled partial differential equations and solved using the finite element method. The problem domain is discretized into four-node linear quadrilateral elements and two node truss elements representing fibers.

Let R_u and R_d denote the residue vectors for the displacement field, u, and the damage field, d, respectively. To solve the coupled system of equations, this work utilizes the staggered algorithm proposed by Gergely et al. [49]. The nonlinear equations are solved iteratively in using the Newton-Raphson method for each equation. The weak form of the equations (7) and (10) that are solved in a staggered manner are

$$R^u = \int_\Omega [B^u]^T\{\sigma\}ds - \int_{\partial\Omega_t} [N^u]^T f da = 0$$

(11)

$$R^d = \int_\Omega \left\{[N^d]^T\left[w'(d)H + \frac{G_c}{c_\alpha l_0}\alpha'(d)\right] + \frac{2l_0 G_c}{c_\alpha}[B^d]^T[B^d]\{d\}\right\}ds = 0$$

(12)

Within the staggered algorithm equations (11) and (12) are solved iteratively at a given pseudo time.

- u_n and d_n represent the known solutions for the displacement and damage fields at the pseudo-time step t_n.
- To find the solution (d_{n+1} and u_{n+1}) at t_{n+1}, the history variable at time t_n (denoted by H_n) is employed to evaluate K_d and R_d. Similarly, d_{n+1} is used to

evaluate K_u and R_u.

- Then u_{n+1} is evaluated iteratively until a pre-defined convergence criterion is satisfied, ensuring the accuracy of the solution.

The concrete and fibers are meshed independently using four-node quadrilateral elements for concrete and two-node linear truss elements for fibers. Let N_f denotes the number of fibers according to the percentage of fiber added in a certain volume. The potential energy of the fibers, denoted by Π_{fib} in Eq. (13), represents the summation of the internal strain energy contribution from each individual fiber. This internal strain energy is calculated along the local coordinate system defined along the length of each fiber. E_f, A_f and L_{iproj} is the young's modulus, area of cross section and projected length of each fiber. $U^{loc}_{fn,i}$ is the component of displacement vector $u^{loc}_{f\,i}$ of ith fiber along the axial length of fiber in the local coordinate system.

$$\Pi_{fib} = \sum_{i=1}^{N_f} \int_0^{L^i_{proj}} \frac{1}{2} E_f A_f \left(\frac{du^{loc}_{fn,i}}{dn_i} \right)^2 dn_i \tag{13}$$

The potential energy of the planar body Ω having boundary $\partial\Omega_u$ and $\partial\Omega_t$ is given as:

$$\Pi = \Pi_e + \Pi_{frac} + \Pi_{fib} + \Pi_{slip}(\|u\|) - \Pi_{ext} \tag{14}$$

Where Π_e, Π_{frac} and Π_{ext} are the strain energy, fracture energy and external work done respectively. The bond slip energy, denoted by $\Pi_{slip}(\|u\|)$, represents the energy dissipated during the debonding process between the fiber and the surrounding concrete matrix. This phenomenon is also referred to as fiber pull-out. The specific expression for the bond slip energy is heavily influenced by the geometry of the fiber (straight, hooked, or corrugated).

To obtain the weak form governing the force balance and damage distribution, the total potential energy, Π, Eq. (14) is minimized with respect to both the displacement field, u_{sc}, and the damage field, d. This directional derivative of energy with respect to u_{sc} and d in admissible directions u_{sc} and d yields two sets of coupled weak form equations, one representing then force equilibrium and the other governing the damage evolution. Mathematically, these equations can be expressed as:

$$\{R^{sc}\} = \left. \frac{\partial\Pi(u_{sc} + \beta\tilde{u}_{sc})}{\partial\beta} \right|_{\beta=0} \tag{15}$$

$$\{R^d\} = \left. \frac{\partial\Pi(d + \beta\tilde{d})}{\partial\beta} \right|_{\beta=0} \tag{16}$$

The set of two coupled equations, Eq. (15) and Eq. (16), are solved iteratively using the staggered algorithm. The computational implementation of these equations is carried out using the embedded truss element of COMSOL Multiphysics software platform.

3.0 RESULTS AND DISCUSSION

The ultimate tensile strength of hybrid rebar is about 1.18 times that of steel rebar (550 MPa) while that of GFRP stirrup is found to be 0.36 times that of steel rebar. The moduli of elasticity of hybrid rebar and GFRP stirrup is only about 0.445 times and 0.0582 times of steel rebar (200 GPa), respectively.

One beam (beam 1) having longitudinal and transverse steel rebars was used as a control beam for comparison with beams reinforced with hybrid rebars for assessing the effectiveness of hybrid rebar in flexure. The control beam was designed as an under-reinforced, flexure critical beam. This beam was designed for an ultimate load of 197.4 kN and it failed at 226 kN. The failure pattern observed was one of diagonal crushing and splitting of concrete at reinforcement level at the supports within the shear span. The shear span / depth ratio for the beam is less than 2. The second beam (Beam 2) having longitudinal hybrid rebars and GFRP as stirrup was designed with a capacity of 181.3 kN. This beam failed at a load of 109.4 kN. The mode of failure was of flexure-shear. Splitting of concrete at the reinforcement level was observed in the shear span. Ultimate failure load has occurred at about 60 percent of the designed load. Stress in hybrid rebar measured at the failure load was 500.14 MPa, which is less than the ultimate stress of hybrid rebar (647 MPa). Failure of beam at lower load is mainly due to slip between the concrete and the rebar. Due to low modulus of elasticity of

hybrid rebars deflection observed is much higher at the same loading stages when compared to the control beam. A third beam (beam 3)was designed for load of 181.3 kN with hybrid rebars as longitudinal reinforcement, GFRP as stirrup and with polypropylene fibers in concrete in order to access the performance of hybrid rebars as longitudinal reinforcement in presence of fibers in concrete. The failure load of this beam was 112.2 kN and the beam failed in flexure-shear mode. Splitting of concrete was observed at the reinforcement level in the shear span. This beam failed at about 61 percent of designed load. Failure at lower load is due to slip between the concrete and rebar. A marginal increment in the load carrying capacity was observed in Beam 3 when compared to the second beam Beam 2 as Beam 3 not had a small dosage of polyester fibers.

The design of hybrid rebar reinforced concrete beams was based on a cover to reinforcement of about 25mm, which is typical of steel reinforced concrete beams. The mode of failure observed in the tests (delamination at the level of reinforcement leading to anchorage failure) in the present investigation suggests that cover to reinforcement is inadequate. This might have led to premature failure of beams, resulting in not realizing the target ductility. Tests on beams reinforced with hybrid rebar have revealed that the failure of the beams was due to loss of bond between rebars and the concrete. Hence the beams did not achieve the target design strengths. An attempt has been made here to develop an analytical model which accounts for loss of bond between rebar and concrete and thus to predict the failure load of beams. The model is based on the bond strength ($_{bond}$) and slip strain (delta$_{slip}$) obtained from the concentric pullout test results. For calculating the development length (L_d) of the rebar in the beam, it is assumed that a critical inclined crack will be formed from the load point and will meet the base of the beam at a distance equal to the effective depth of the beam from the loading point by trial-and-error process, neutral axis depth $'x'$ is determined. Upon determining 'x', failure moment and load are computed. The

predicted failure load for beams beam 2 and beam 3 is found to be 94.9kN. Predicted failure load is in satisfactory agreement with the experimental failure load (109 kN for Beam 2 and 112KN for Beam 3 .

Given the inherent randomness in fiber distribution within the concrete matrix, it is essential to assess the model's sensitivity to fiber placement. Four different random fiber distributions are generated for a constant fiber volume fraction of 0.5% (Figure 1).

A refined mesh of four node quadrilateral element of size 1.67 mm (i.e, one third of the l_0 value) is employed in the vicinity of the notch to accurately capture the crack initiation and propagation in the three-point bend specimen (400mm long, 100mm deep, clear span of 300mm and notch depth of 25mm). The material properties for the plain concrete are defined as follows: Young's modulus (E) = 29.9 GP a, Poisson's ratio (ν) = 0.2, tensile strength (ft) = 4.00 MP a, fracture energy (G$_c$) = 0.25 N/mm, and characteristic length scale (l_0) = 5 mm. The numerical solution is obtained through an incremental loading scheme using the Newton-Raphson method with a displacement increment of 0.0002 mm.

Figure 1 illustrates the damage distribution for these sample realizations, revealing varying numbers of fibers bridging the crack. The simulated crack path is consistent with the experimental observations [35]. The crack in experiment always initiates from the notch [37, 48] and propagates in transverse direction across the cross section similar trends has been captured in the simulation done by present model. The corresponding load-displacement curves, presented in figure 2, demonstrate consistent pre-peak behavior but exhibit variations in the post-peak response for the four realizations of fiber distribution. These observations align with experimental findings reported by Yoo et al. [35], which indicate a similar degree of variability in post-peak behavior due to random fiber distribution. However, present model predicted the behaviour of SFRC near to the upper bound of experimental finding as shown in figure 2.

The predicted peak load varies between 7.2 kN and 7.5 kN for different fiber distributions

within the model. These values are comparable to the mean experimental peak load of 6.46 kN
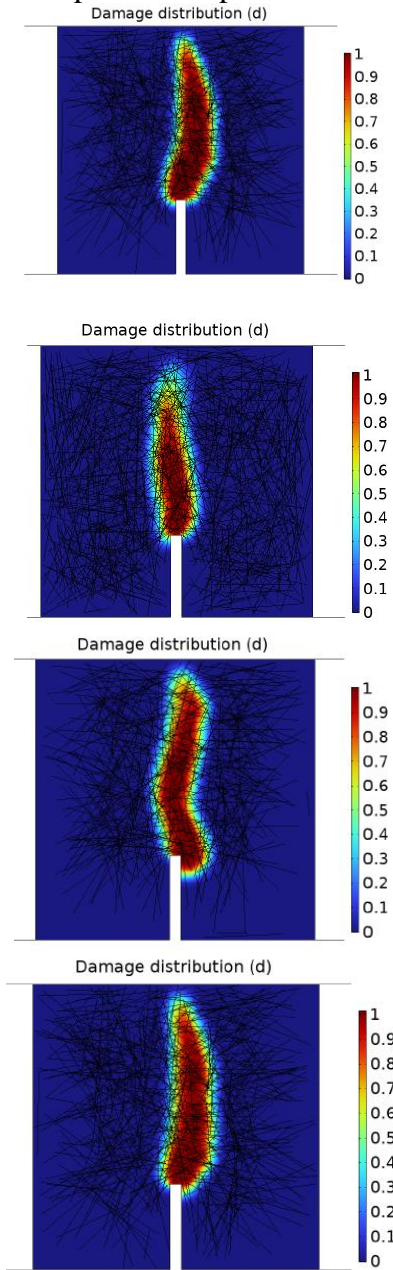
Figure 1 Damage contours for different realisations of random distribution of fibers.

with a standard deviation of 0.48 kN, [35]. Furthermore, the post-peak behavior captured by the model aligns well with the experimental observations. Figure 3 illustrates the fiber strain distribution within the fully cracked specimen. The results indicate that fibers near the crack experience significantly higher strains compared to those located further away. This observation validates the model's ability to capture the critical phenomenon of

crack bridging.
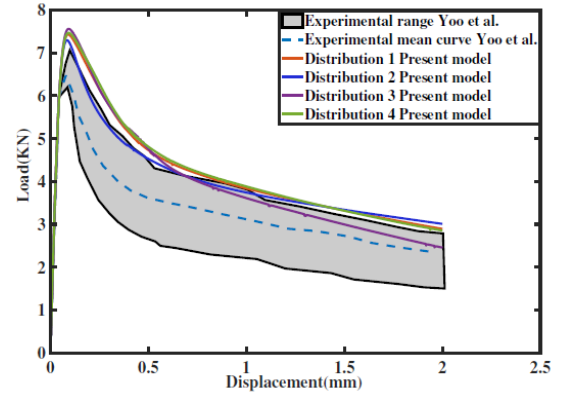
Figure 2 Comparison of load-deflection curve of present model for 0.5% fiber content and experimental observation [35]

4.0 CONCLUSIONS

The study of hybrid rebars shows promise but issues such as bond strength and cover need to be carefully examined to enhance the capacity. This study proposed a multi-scale approach to simulate the fracture behavior of Steel Fiber Reinforced Concrete (SFRC) where the concrete matrix is modelled at the macro- scale, while individual fibers are explicitly considered in the model. The fibers are randomly distributed within the 3D domain, with a focus on regions susceptible to crack initiation. The model employs a phase-field-based quasi-brittle damage law to describe the behavior of concrete, whereas a linear elastic behaviour is assumed for the fibres. The interaction between fibers and the concrete matrix is represented through a bond-slip model. Afterwards, the numerical results, such as load capacity or peak load, post-peak behavior, and crack patterns are compared with the available experimental data. Based on study performed, the following conclusions can be drawn:

- The comparison of proposed model predictions with experimental results suggests that the current macroscale modelling approach of concrete matrix is sufficiently accurate. Hence coarse aggregate has minimal effects on the global fracture response of SFRC.
- Analysing the detailed results, such as damage evolution within the concrete matrix, strains within the fibers, and

internal forces acting on the fiber-matrix interface, can be leveraged to conduct numerical experiments to optimize the material's composition and design parameters that meet the specific performance requirements reducing the need for extensive experimental testing.
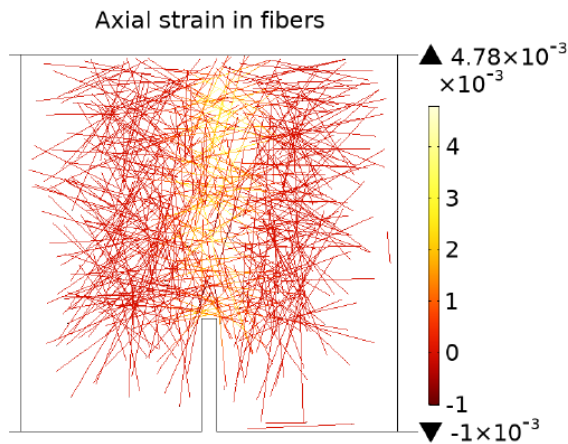
Figure 3 Axial strain in the fibers for a fully cracked specimen

5.0 REFERENCES

[1] Sonobe, Y., Fukuyama, H., Okamoto, T., Kani, N., Kimura, K., Kobayashi, K., Masuda, Y., Matsuzaki, Y., Mochizuki, S., Nagasaka, T., Shimizu, A., Tanano, H., Tanigaki, M., and Teshigawara, M., 'Design guideline s of FRP reinforced concrete building structures', *Journal of Composites' for Construction, ASCE* 1 (4) (1997) 90-114.

[2] Yost, J.R., Gross, S.P. and Dinehart, D.W., 'Shear strength of normal strength concrete beams reinforced with deformed GFRP bars', *Journal of Composites for Construction, ASCE* 5 (4) (2001) 268-275.

[3] Kuntia, M., Stojadinovic, B. and Goel, S.C., 'Shear strength of normal and high-strength fiber reinforced concrete beams without stirrups', *ACI Structural Journal 96* (2) (1999) 282-289.

[4] Biswarup Saikia, Phanindra Kumar, Job Thomas, K.S. Nanjunda Rao, Ananth Ramaswamy Strength and serviceability performance of beams reinforced with GFRP bars in flexure *Construction and Building Materials* 21 (2007) 1709–1719

[5] B. Pal, A. Ramaswamy, A multi-physics-based approach to predict mechanical behavior of concrete element in a multi-scale framework, *Mechanics of Materials* 176 (2023) 104509.

[6] Hughes, B.P., Design of prestressed fiber reinforced concrete beams for impact," *ACI Journal,* Vol.78, No.4, Jul.-Aug., pp.276-281.

[7] Narayanan, R, and Kareem-Palanjian, A.S., (1984), "Torsion in prestressed concrete beams containing steel fibers," *The International Journal of Cement Composites and Lightweight Concrete,* Vol.16, No.2, May, pp.81-91.

[8] Narayanan, R., and Darwish, I.Y.S., (1987), "Shear in prestressed concrete beams containing steel fibers," *The International Journal of Cement Composites and Lightweight Concrete*, Vol.9, No.2, May, pp.81-90.

[9] Balaguru, P.N., Ezeldin, A., (1987), "Behavior of partially prestressed beams made with high strength fiber reinforced concrete," *Fiber Reinforced Concrete Properties and Application SP-105*, Shah S.P. and Batson G.B. eds., American Concrete Institute, pp.419-436.

[10] Wafa, F.F., Hasanat, A., and Tarabolsi, O.F., (1992), "Prestressed fiber reinforced concrete beams subjected to torsion," *ACI Structural Journal*, Vol.89, No.3, May-Jun., pp.272-283.

[11] Tan, KH., Paramasivam, P., and Murugappan, K., (1995), "Steel fiber as shear reinforcement in partially prestressed beams," *ACI Structural Journal,* Vol.92, No.6, Nov.-Dec., pp.643-652.

[12] diPrisco, M., and Cambarovam P.G., (1995), "Comprehensive model for study of shear in thin webbed RC and PC beams," *Journal of Structural Engineering, ASCE*, Vol.121, No.12, Dec., pp.1822-1831.

[13] Furlan, Jr., S., and de-Hanai, J.B., (1999), "Prestressed fiber reinforced concrete beams with reduced ratio of shear reinforcement," *Cement and Concrete*

Composites, Vol.21, No.2, pp.213-221.

[14] Abdul-Wahab, H.M.S., and Al-Kadhimi, S.G., (2000), "Effect of SFRC on shear strength of prestressed concrete beams," *Magazine of Concrete Research*, Vol.52, No.1, Feb., pp.43-51.

[15] Padmarajaiah, S.K. and Ramaswamy, A., (2002), "Flexural strength predictions of steel fiber reinforced high strength concrete in fully / partially prestressed beam specimens," *Cement and Concrete Composites*, Vol.24, No.2, pp.229-241.

[16] Padmarajaiah, S.K., and Ramaswamy, A., (2001), "Crack width Prediction of high strength concrete fully and partially prestressed beam specimens containing steel fibers," *ACI Structural Journal*, Vol.98, No.6, Nov.-Dec., pp.852-861.

[17] Thomas J., and Ramaswamy, A. "Mechanical Properties of SFRC", *ASCE Material in Civil Engineering,* 19(5) 385-392, 2007.

[18] Tan, KH., Paramasivam, P., and Murugappan, K., (1995), "Steel fiber as shear reinforcement in partially prestressed beams," *ACI Structural Journal,* Vol.92, No.6, Nov.-Dec., pp.643-652.

[19] Chern, JC., Yang, HJ., Chen, HW., (1992), "Behavior of steel fiber reinforced concrete in multiaxial loading," ACI *Materials Journal*, Vol.89, No.1, Jan.-Feb., pp.32-40.

[20] Z. Hashin, S. Shtrikman, A variational approach to the theory of the elastic behaviour of multiphase materials, *Journal of the Mechanics and Physics of Solids* 11 (1963) 127–140.

[21] R. Hill, The elastic behaviour of a crystalline aggregate, *Proceedings of the Physical Society. Section A* 65 (1952) 349.

[22] J. D. Eshelby, The determination of the elastic field of an ellipsoidal inclusion, and related problems, *Proceedings of the royal society of London. Series A. Mathematical and physical sciences* 241 (1957) 376–396.

[23] M. Congro, F. Pereira, L. Souza, D. Roehl, A hybrid parameter homogenization workflow for assessing the mechanical behavior of a steel fiber-reinforced concrete, *Mechanics of Composite Materials* 59 (2024) 1157–1168.

[24] T. Mori, K. Tanaka, Average stress in matrix and average elastic energy of materials with misfitting inclusions, *Acta metallurgica* 21 (1973) 571–574.

[25] S. Nemat-Nasser, M. Hori, Micromechanics: overall properties of heterogeneous materials, Elsevier, 2013.

[26] R. Christensen, K. Lo, Solutions for effective shear properties in three phase sphere and cylinder models, *Journal of the Mechanics and Physics of Solids* 27 (1979) 315–330.

[27] K. Babu, P. Mohite, C. Upadhyay, "Development of an rve and its stiffness predictions based on mathematical homogenization theory for short fibre composites," *International Journal of Solids and Structures* 130 (2018) 80–104.

[28] F. Deng, X. Ding, Y. Chi, L. Xu, L. Wang, "The pull-out behavior of straight and hooked-end steel fiber from hybrid fiber reinforced cementitious composite: Experimental study and analytical modelling", *Composite Structures* 206 (2018) 693–712.

[29] L. A. Bitencourt Jr, O. L. Manzoli, T. N. Bittencourt, F. J. Vecchio, Numerical modeling of steel fiber reinforced concrete with a discrete and explicit representation of steel fibers, *International Journal of Solids and Structures* 159 (2019) 171–190.

[30] M. Cervera, J. Oliver, O. Manzoli, "A rate-dependent isotropic damage model for the seismic analysis of concrete dams", *Earthquake engineering & structural dynamics* 25 (1996) 987–1010.

[31] L. A. Bitencourt Jr, O. L. Manzoli, P. G. Prazeres, E. A. Rodrigues, T. N. Bittencourt, A coupling tech- nique for non-matching finite element meshes, *Computer methods in applied mechanics and engineering* 290 (2015) 19–44.

[32] Y. T. Trindade, L. A. Bitencourt Jr, R.

Monte, A. D. de Figueiredo, O. L. Manzoli, Design of sfrc members aided by a multiscale model: Part i–predicting the post-cracking parameters, *Composite Structures*, 241 (2020) 112078.

[33] M. Hafezolghorani, F. Hejazi, R. Vaghei, M. S. B. Jaafar, K. Karimzade, Simplified damage plasticity model for concrete, *Structural engineering international*, 27 (2017) 68–78.

[34] H.-L. Minh, S. Khatir, M. A. Wahab, T. Cuong-Le, A concrete damage plasticity model for predicting the effects of compressive high-strength concrete under static and dynamic loads, *Journal of Building Engineering*, 44 (2021) 103239.

[35] D.-Y. Yoo, Y.-S. Yoon, N. Banthia, Predicting the post-cracking behavior of normal-and high-strength steel-fiber-reinforced concrete beams, *Construction and Building Materials*, 93 (2015) 477–485.

[36] B. Li, L. Xu, Y. Shi, Y. Chi, Q. Liu, C. Li, Effects of fiber type, volume fraction and aspect ratio on the flexural and acoustic emission behaviors of steel fiber reinforced concrete, *Construction and Building Materials*, 181 (2018) 474–486.

[37] D.-Y. Yoo, Y.-S. Yoon, N. Banthia, Flexural response of steel-fiber-reinforced concrete beams: Effects of strength, fiber content, and strain-rate, *Cement and Concrete Composites*, 64 (2015) 84–92.

[38] J.-Y. Wu, A unified phase-field theory for the mechanics of damage and quasi-brittle failure, *Journal of the Mechanics and Physics of Solids*, 103 (2017) 72–99.

[39] C. Miehe, M. Hofacker, F. Welschinger, A phase field model for rate-independent crack propagation: Robust algorithmic implementation based on operator splits, *Computer Methods in Applied Mechanics and Engineering*, 199 (2010) 2765–2778.

[40] Y. Xia, W. Wu, Y. Yang, X. Fu, Mesoscopic study of concrete with random aggregate model using phase field method, *Construction and Building Materials*, 310 (2021) 125199.

[41] P. Zhang, X. Hu, S. Yang, W. Yao, modelling progressive failure in multi-phase materials using a phase field method, *Engineering Fracture Mechanics*, 209 (2019) 105–124.

[42] P. Zhang, X. Hu, S. Yang, W. Yao, modelling progressive failure in multi-phase materials using a phase field method, *Engineering Fracture Mechanics* 209 (2019) 105–124.

[43] W.-X. Chen, J.-Y. Wu, Phase-field cohesive zone modeling of multi-physical fracture in solids and the open-source implementation in COMSOL Multiphysics, *Theoretical and Applied Fracture Mechanics*, 117 (2022) 103153.

[44] Zhang, J.-G. Dai, C. S. Das, J.-J. Zheng, A fully coupled meso-scale electro-chemo-mechanical phase field method for corrosion-induced fracture in concrete, International *Journal of Solids and Structures*, 267 (2023) 112165.

[45] P. Soroushian, C.-D. Lee, Distribution and orientation of fibers in steel fiber reinforced concrete, *ACI Materials journal*, 87 (1990) 433–439.

[46] J. Han, M. Zhao, J. Chen, X. Lan, Effects of steel fiber length and coarse aggregate maximum size on mechanical properties of steel fiber reinforced concrete, *Construction and Building Materials*, 209 (2019) 577–591.

[47] V. M. Cunha, J. A. Barros, J. M. Sena-Cruz, A finite element model with discrete embedded elements for fiber reinforced composites, *Computers & structures*, 94 (2012) 22–33.

[48] B. Li, L. Xu, Y. Shi, Y. Chi, Q. Liu, C. Li, Effects of fiber type, volume fraction and aspect ratio on the flexural and acoustic emission behaviors of steel fiber reinforced concrete, *Construction and Building Materials*, 181 (2018) 474–486.

[49] G. Molnar, A. Gravouil, 2d and 3d abaqus implementation of a robust staggered phase-field solution for modelling brittle fracture, *Finite Elements in Analysis and Design* 130 (2017) 27–38.